J.Serb.Chem.Soc. 68(3)191–205(2003)
JSCS – 3034

UDC 66.087.3:546.263.3–34+546.92
Original scientific paper

Electrochemical oxidation of carbon monoxide: from platinum single crystals to low temperature fuel catalysts. Part II: Electrooxidation of H_2, CO and H_2/CO mixtures on well characterized PtMo alloy

BRANIMIR N. GRGUR[1,* #], NENAD M. MARKOVIĆ[2] and PHILIP N. ROSS JR.[2]

[1]*Faculty of Technology and Metallurgy, University of Belgrade, Karnegijeva 4, 11001 Belgrade, Serbia and Montenegro and* [2]*Lawrence Berkeley National Laboratory, 1 Cyclotron Road, MS 2-100, Berkeley, CA 94720, USA*

(Received 5 November 2002)

Abstract: The oxidation of hydrogen and hydrogen–carbon monoxide mixture has been investigated on well-characterized metallurgically prepared platinum–molybdenum (PtMo) alloys. It was concluded that the optimum surface concentration of molybdenum is near 23 mol.%. Based on experimentally determined parameters and simulations, the mechanism of the oxidation of CO/H_2 mixtures is discussed.

Keywords: fuel cell, anode, platinum, molybdenum, hydrogen, carbon monoxide.

INTRODUCTION

In a previous paper, the oxidation of carbon monoxide on a well-defined single crystal platinum electrode was investigated.[1] It was concluded that for fuel cell applications it is important to release the platinum atoms of the CO_{ads} on which the oxidation of hydrogen reaction can occur. The mechanism of hydrogen oxidation in H_2/CO mixtures on platinum was given by the following sequence of reactions:

$$CO_b + Pt \xrightarrow{k_{ads}(CO)} Pt\text{–}CO_{ads} \quad (1)$$

$$Pt + H_2O \underset{\leftarrow}{\overset{\rightarrow}{}} Pt\text{–}OH_{ads} + H^+ + e^- \quad (2)$$

$$Pt\text{–}CO_{ads} + Pt\text{–}OH_{ads} \xrightarrow{k_{ox}(CO)} CO_2 + H^+ + 2Pt + e^- \quad (3)$$

$$2Pt + H_2 \rightarrow 2Pt\text{–}2H_{ads} \quad (4)$$

* Corresponding author: e-mail: BNGrgur@elab.tmf.bg.ac.yu.
\# Serbian Chemical Society active member.

$$2Pt–2H_{ads} \rightarrow 2Pt + 2H^+ + 2e^- \quad (5)$$

The hydrogen oxidation reaction occurs on the free sites liberated during the time between the oxidative removal of CO_{ads}, Eq. (3) and CO readsorption from solution, Eq. (1). At low potentials ($E < \approx 0.6$ V), the rate constant of CO_b readsorption is much higher then the rate constant for CO_{ads} oxidation and practically only an infinitely small number of platinum sites could be liberated for H_2 oxidation. The hydrogen oxidation reaction reaches a maximum at the same potential where CO_{ads} is oxidized by Pt–OH (coverage with CO_{ads} in that potential region tends to zero). According to this, it is necessary to provide a supply of OH species to adjunct platinum atoms covered by CO_{ads} by some other metal which does not adsorb CO. This type of catalyst is known as a bi-functional catalyst.[2] A schematic representation of such a catalyst is given in Fig. 1.

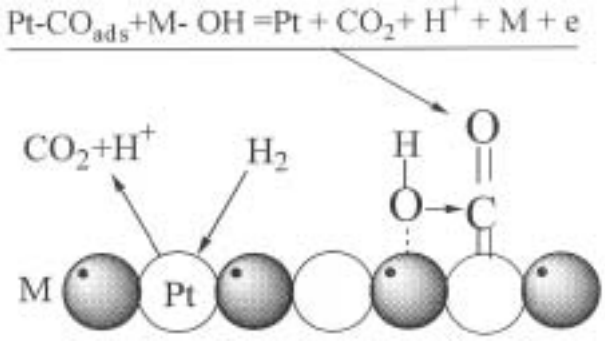

Fig. 1. Bi-functional catalyst (schematic representation).

As the alloying metal (M) should provide OH (note: at the present the nature of "OH" on M is not known) for the reaction with CO_{ads}:

$$Pt–CO_{ads} + OH–M \rightarrow Pt + M + CO_2 + H^+ + e^- \quad (6)$$

it is necessary to find such a metal which can provide OH at a low as possible potential (*e.g.*, near the hydrogen reversible potential). Although, practically, all transition metalis are oxidized in acid solutions, the fact is that only a few metals in an alloy with platinum shows certain activity for the oxidation of H_2/CO mixtures. The polarization curves for 2 % CO and 2 % CO/H_2 mixtures on Pt, PtRu, Pt_3Sn and Pt_3Re electrodes are shown in Fig. 2.[3] It is obvious that H_2 oxidation follows CO oxidation, which is in agreement with the above given discussion. A Pt_3Re alloy shows activity similar to platinum, while PtRu and Pt_3Sn alloys are much better catalyst, but the potential loss is still to high, 0.4 V and 0.3 V, respectively. PtRu is, in fact, not a real CO bi-functional catalyst, because Ru also adsorbs CO and provides OH (as oxy-hydroxide) in the potential range above 0.4 V. On the other hand, PtSn alloy is the best known real catalyst for CO oxidation but, unfortunately, this alloy is corrosion unstable and during the time Sn dissolves from the surface layer. The inactivity of different Pt–M alloys could be searched for in the metal to oxygen bond strength and in the corrosion behavior of the alloys. Electronegative alloying metals, such as Ti, V,

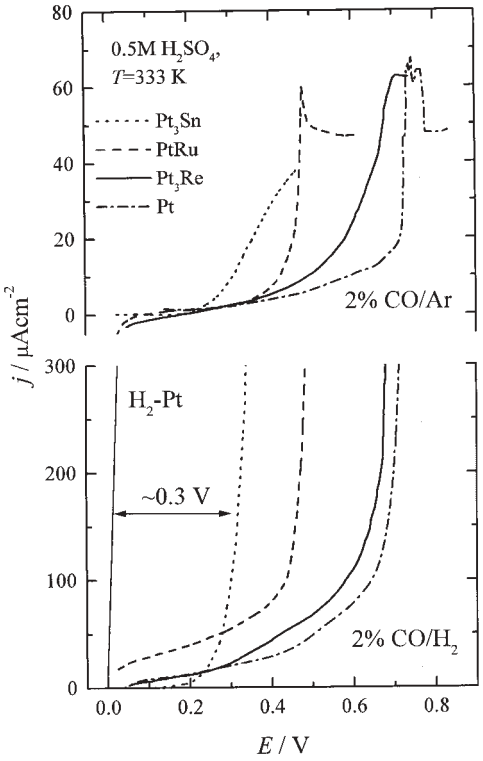

Fig. 2. Polarization curves (1 mV s^{-1}) for the oxidation of 2 % CO in argon (upper), and 2 % CO in hydrogen (lower) on different catalysts in 0.5 M H_2SO_4 at 2500 rpm, 333 K.

Nb, Ta, *etc.*, have a too strong a bond strength (practically in the form of the metal oxides) so these metals cannot provide oxygenated species for CO_{ads} oxidation. Some noble metals could provide oxygenated species which can oxidize CO_{ads} (*e.g.*, Ru, Ir, Au) but the potential where these metals are in the form of oxy-hydroxides is too high for application as the anode in fuel cells. On the other hand, the transition metals (Fe, Co, Ni, Mn) and some other metals and metalloids, such as Zn, Cd, Ga, Bi, In, Sb, Ge, *etc.*, are in the form of oxy-hydroxide at low potentials ≈ 0 V *vs.* RHE, but unfortunately most of the platinum alloys with these metals are corrosion unstable or during the thermal preparation of the alloys strong segregation and enrichment in platinum in to the surface layer occurs, resulting in alloys with platinum like behavior. By analyzing the metal to oxygen bond strength and thermodynamic data of metal oxidation in acid solution,[4–6] it was concluded that platinum alloys with molybdenum or tungsten could be the metal of choice. Platinum–molybdenum alloy was chosen for further investigation, mostly because the melting point of tungsten is too high (3410 ºC) and so it is difficult to prepare an alloy with platinum.

EXPERIMENTAL

Polycrystalline platinum–molybdenum alloys were prepared by two different methods. The first of these methods was the conventional metallurgical technique of arc melting of the pure elements in an argon atmosphere followed by a homogenizing heat treatment in vacuum. The bulk composition of the alloy was 66 mol.% Pt and 33 mol.% Mo. The second method involved high-dose ion implantation of Mo into a polycrystalline platinum sample by plasma immersion-ion implantation. In this method, the substrate (Pt) is

immersed in a plasma of the desired implantation species (Mo) and repetitively pulse-biased to a high negative voltage. A high voltage sheath rapidly forms at the plasma-substrate boundary and plasma ions are accelerated through the sheath and into the substrate (for details see Refs. 7 and 8).

Before UHV characterization, the metallurgically prepared Pt_3Mo alloy was mechanically polished with a diamond and Al_2O_3 (0.05 μm) slurry to an optically flat surface, followed by ultrasonic cleaning in 3 M KOH and bidistiled water. The ion implanted sample was ultrasonically cleaned in methanol and then in bidistiled water.

The PtMo alloys were characterized by means of the AES (Auger electron spectroscopy), XPS (X-ray photoelectron spectroscopoy) and LEIS (low energy ion scattering) techniques. Data were collected using an angle-resolving double pass cylindrical mirror analyzer. For LEIS, a 2 keV He^+ ion beam was restarted over a 3 mm × 3 mm area of the surface at an incident angle of 45º. The average scattering angle, θ was 127º with resolution less than 1º. A conventional laboratory X-ray source was used with a Mg twin-anode. Calibration of the LEIS sensitivity factors and the XPS binding energies was carried out using pure Pt and Mo polycrystals. The composition of the surface of the alloys was determined by means of LEIS. The metallurgically prepared alloy had two different compositions depending of the finishing treatment. After treatment by annealing at 970 K for 30 min, the resulting surface concentration of Mo was 23 mol.%, and after Ar ion (0.5 keV) sputtering 30 mol.%. The equilibrium surface composition of the plasma implanted alloy was 15 mol.% Mo.

After UHV characterization, the electrode, (A = 0.283 cm^2), was mounted in the disk position of the RDE assembly following the same procedure as for platinum single crystals.

In all experiments, a 0.5 M H_2SO_4 (ULTREX II, J. T. Baker Reagent) solution, prepared with triply distilled water, was used. All potentials are referenced to the reversible hydrogen electrode (RHE) in the same solution and at the same temperature. a circulating constant temperature bath (Fisher Isotemp Circulator) maintained the temperatures of the solutions within ± 0.5 K. A Pine Instruments Bipotentiostat (Model AFRDE 4; potential response 0.5 V/ms) was used for all the experiments. Pure (5N8) CO, CO/H_2, CO/Ar, and CO_2 gasses were purchased from Matheson.

RESULTS AND DISCUSSION

Surface characterization of the platinum–molybdenum alloys

Typical AES and LEIS spectra for the Pt_3Mo alloy surface after numerous cycles of Ar ion sputtering (0.5 keV) and thermal annealing (970 K for 30 min) are shown in Fig. 3. AES analysis was conducted only for the purpose of assessing the surface cleanliness. The trace amounts of carbon and oxygen remaining on the surface, however, were considered not to affect the LEIS analysis or the electrochemical properties of the surface. Typical LEIS spectra for annealed and sputtered surfaces are shown in the insert in Fig. 3. The peak energies for Pt and Mo agreed to within ±0.5 % with the values predicted by the classical equation for elastic collisions[9]:

$$\frac{E_1}{E_0} = \frac{M(\mathrm{He})^2}{[M(\mathrm{He}) + M(\mathrm{Pt})]^2}\left[\cos\theta + \sqrt{\left(\frac{M(\mathrm{Pt})^2}{M(\mathrm{He})^2} - \sin^2\theta\right)}\right]^2 \qquad (7)$$

where M is the molar mass of helium, platinum or molybdenum, θ is the average scattering angle (127º), E_0 the energy of helium ions 2 keV and E_1/E_0 is the peak position of the element (Pt or Mo).

The surface composition, x, was calculated from the peak heights, H_{Pt} and H_{Mo}, determined by fitting the spectrum with Gaussian profiles, according to:

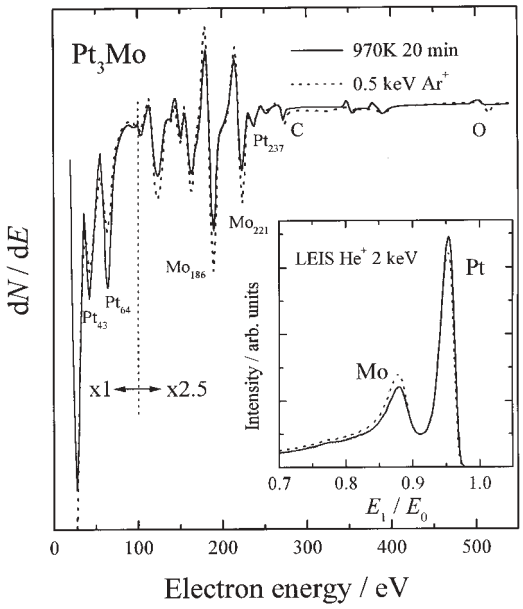

Fig. 3. Derivative mode ASE spectrum of the Pt_3Mo alloy following sputter-cleaning and annealing at 970 K. Insert LEIS spectra of the same surface.

$$x_{Mo} = S_{Mo/Pt}H_{Mo}/(S_{Mo/Pt}H_{Mo} + H_{Pt}) \quad (8)$$

where $S_{Mo/Pt}$ is the sensitivity factor on an atomic basis, defined as:

$$S_{Mo/Pt} = (I_{Mo}/I_{Pt})(a_{Pt}/a_{Mo})^2 \quad (9)$$

where I is the peak height of the pure elements under the same experimental conditions, and a is the lattice constant.[10] The surface composition for the annealed sample was 23 mol.% Mo, while the sputtered surface was 30 mol.% Mo, nominally identical to the bulk composition.

TABLE I. Core-level, binding energies and chemical shifts for clean, annealed PtMo alloy

	Binding energy/eV			
	$3d_{5/2}$	$3d_{3/2}$	$3p_{3/2}$	$3p_{1/2}$
Mo	227.8	231.0	394.0	411.5
$Mo_{(PtMo)}$	227.3	230.5	393.8	411.3
Shift/eV	– 0.5	– 0.5	– 0.2	– 0.2
	$4f_{7/2}$	$4f_{5/2}$	$4d_{5/2}$	$4d_{3/2}$
Pt	71.1	74.4	315.0	331.8
$Pt_{(PtMo)}$	71.4	74.7	314.8	331.6
Shift/eV	+0.3	+0.3	+0.2	+0.2

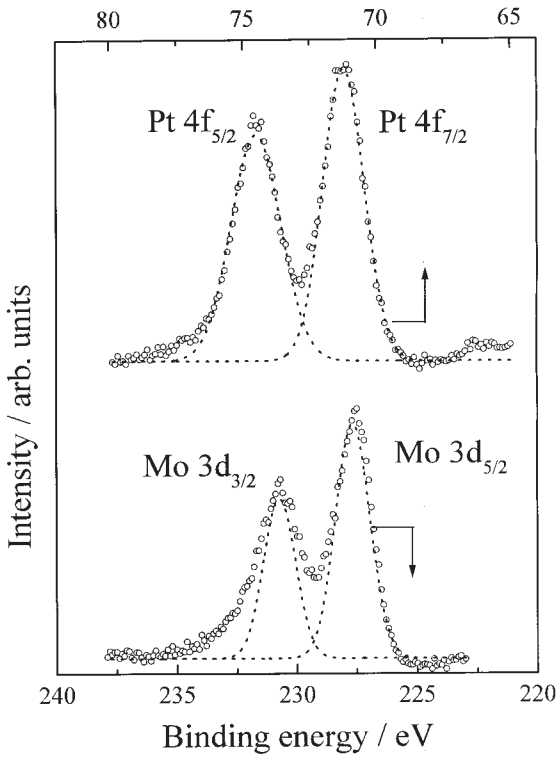

Fig. 4. XPS spectra from the Pt 4f (upper) and Mo 3d (lower) core-levels for the annealed surface from Fig. 3. Dashed lines curve fitting and deconvolution (after background subtraction) of the spectrum.

The core level binding energies for Mo 3d, 3p and Pt 4f and 4d orbitals were determined from high-resolution XPS spectra (examples for Mo 3d and Pt 4f doublet orbitals are shown in Fig. 4). The binding energies for the characteristic core levels are summarized in Table I. The chemical shifts relative to the pure metals indicate the charge transfer from Mo to Pt atoms, which occurs to a lesser extent than in Pt_3Sn or Pt_3Ti alloys, where the bonding has a strongly ionic character with the Sn(Ti) atom being nearly in a cationic state.[11] According to the calculation of Miedema,[12] the intermetallic bonding is relatively storng in the PtMo alloy, being intermediate between the highly exothermic alloys Pt_3Sn or Pt_3Ti and the slightly endothermic alloy PtRu. The chemical shifts indicate that the molybdenum atoms are stabilized in the alloy, which can have a further effect on the electrochemical behavior of the electrode.

With the same analysis performed for the Pt_3Mo bulk alloy, the equilibrium surface composition of the plasma implanted PtMo alloy with 15 mol.% Mo, was determined (for details see Ref. 13).

After surface characterization, the sample was transferred from the UHV chamber into an electrochemical cell.

Electrochemical characterization

Cyclic voltammetry of PtMo and the hydrogen oxidation reaction. The voltammetric profiles of the $Pt_{70}Mo_{30}$, $Pt_{77}Mo_{23}$ and $Pt_{85}Mo_{15}$ surfaces in 0.5 M H_2SO_4, together with pure platinum samples are shown in Fig. 5. The voltammograms were recorded immediately following transfer from the UHV chamber into argon purged 0.5 M H_2SO_4. The upper potential limit of 0.85, 0.65 and 0.45 V for $Pt_{70}Mo_{30}$, $Pt_{77}Mo_{23}$ and $Pt_{85}Mo_{15}$, respectively, were chosen in order to avoid possible Mo dissolution from the surface. A distin-

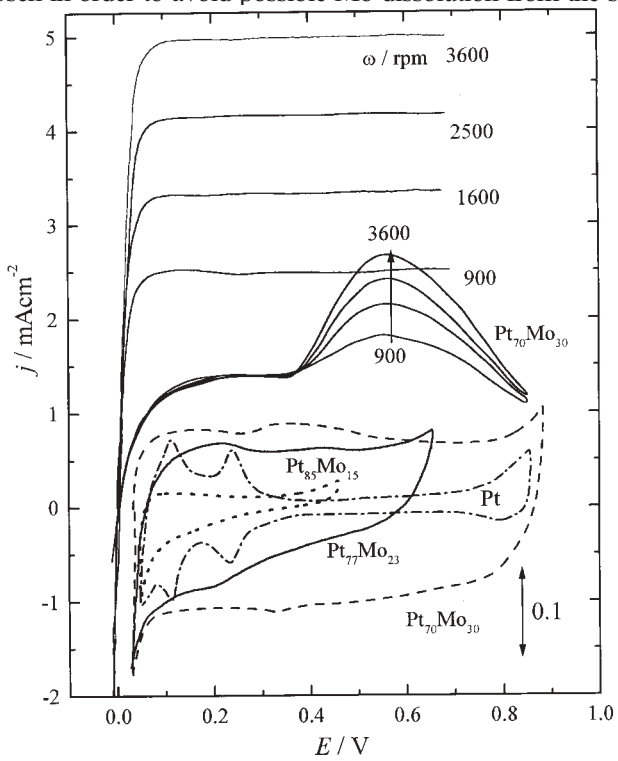

Fig. 5. (Lower) Cyclic voltammograms (50 mV s^{-1}) in deaerated 0.5 M H_2SO_4 of the different surfaces (marked in the Figure). Polarization curves (1 mV s^{-1}) in H_2 saturated electrolyte at 333 K at different rotation rates (upper).

guishing characteristic in the voltammetry of PtMo surfaces, from the well-known voltammetric features of a Pt electrode, is that the H_{upd} region is not well defined on these surfaces. In fact, the voltammetry of the $Pt_{70}Mo_{30}$, surface shows a huge capacitance over the whole investigated potential region. Between ≈ 0.2 and 0.6 V, a broad peak, connected with Mo oxidation/reduction, can be seen. There is no increase of the current below 0.8 V which would indicate Mo dissolution from the electrode. The cyclic voltammogram of the $Pt_{77}Mo_{23}$ electrode is similar as that for a pure Mo electrode.[13] In the positive going sweep direction, a broad shoulder, which was observed at ≈ 0.1 V, is followed by two peaks, the first one at 0.23 V and the second one at ≈ 0.45 V. The voltammetric profile of the

$Pt_{85}Mo_{15}$ surface in 0.5 M H_2SO_4 solution has a more ruthenium like than a Pt-like behavior. The only two characteristics of this surface were an increase of the current above 0.4 V in the anodic sweep direction, and an indication of a reduction peak in the potential region between 0.1– 0.2 V. The increase of the current above 0.4 V could not be unconditionally connected only with Mo dissolution from the surface layer but also with the redox processes observed on the other two surfaces in the same potential region. Since the sample had only a limited amount of Mo in the surface layer, any loss would make it impossible to restore the surface by simple reconditioning in the UHV chamber, as with the other surfaces, so the positive potential limit was restricted to prevent any possible loss of Mo from the surface layer. The charge of the $Pt_{85}Mo_{15}$ electrode in the H_{upd} region was much smaller than in the case of a pure platinum electrode, which could mean that Mo atoms suppress the hydrogen underpotential deposition reaction. Such a decrease of the charge in the H_{upd} region could not be simply explained by a geometric effect of the molybdenum atoms in the surface layer (corresponding charge for 15 mol.% of Mo is ≈180 μC cm^{-2}). A more reasonable explanation is that Mo is already oxidized at low potentials, and that the oxygen containing species from one Mo atom block more than one Pt atom. Based on this supposition, it can be concluded that the charge of a PtMo electrode in the investigated potential region is mostly connected with the molybdenum oxidation/reduction reaction. According to this, the non-linear increase of the electrode charge with increasing Mo concentration means that even in the low potential region, Mo is oxidized, probably as Mo(III) oxi-hydroxide species, and that an increase of Mo in the surface by one atom increases the charge of the electrode by a minimum of 3e. In the higher potential region, $0.25 < E < 0.55$, Mo is probably in the Mo(IV) oxidation state, and at the higher potentials more positive than 0.6 V, Mo is in the Mo(VI) or Mo(VIII) oxidation state, but dissolution in the form of H_2MoO_4 is prevented by the stabilization of Mo atoms in the alloy.

A first condition for the use of a catalyst in a fuel cell anode is good catalytic properties in the hydrogen oxidation reaction. After recording the cyclic voltammograms, the solution was saturated with H_2 and the hydrogen oxidation reaction was examined, as shown in Fig. 5. At $Pt_{85}Mo_{15}$ and $Pt_{77}Mo_{23}$ electrodes, the reaction rates are identical with the rate of oxidation of hydrogen on a pure Pt electrode, the polarization curves of which are also shown in Fig. 5 for comparison. The overpotential/current relation closely follows that for pure diffusion control:

$$\eta = -2.303(RT/2F) \log (1 - j/j_d) \quad (10)$$

where j_d is the measured diffusion-limited current density at any rotation rate and j is the observed current density at an overpotential η. The slope of 8.2×10^{-2} mA cm^{-2} $(rpm)^{-1/2}$ at $E = 0.1$ V, in the $j - \omega^{1/2}$ plot (not shown), has practically the theoretical value.[14] While a relatively small surface concentration of Mo (15 and 23 mol.%) atoms has no effect (practically unmeasurable by standard RDE methods) on the hydrogen oxidation reaction, the HOR is, however, dramatically inhibited on the $Pt_{70}Mo_{30}$ surface. Figure 5 shows that below 0.4 V the polarization curve is practically independent of the rotation rate which is atypical for pure diffusion control. This implies reaction control with probably a Tafel

(chemical) reaction as the rate-determining step. Above 0.4 V, some increase of the current density and a dependence on the rotation rate was observed, but more likely as mixed diffusion–reaction control. Above 0.6 V, the current density decreases again which is connected with the oxidation of Pt atoms on the surface. This dramatic change in the shape of the polarization curve is strongly connected with the surface chemistry of the Mo atoms at the surface. The change of the reaction rate at 0.4 V occurs at the same potential as the observed peak in cyclic voltammogram. This could imply that below 0.4 V, Mo is in the form of $Mo(OH)_3$ and above 0.4 V in the form of MoO_2 and at the more positive potential as MoO_3 and/or $MoO_2(OH)_2$. Such a hypothesis is given by the fact that $Mo(OH)_3$ is geometrically a much bigger surface species than MoO_2 and as a result could block more platinum atoms than the smaller MoO_2. The electrochemistry of Mo is extremely complicated (more than thirty different reactions in the potential range from – 0.2 to 0.4 V (SVE) are possible[5,6]), so it is impossible to know in which form Mo is present in the surface at any given potential, especially since at the same potential the coexistence of atoms with different oxidation states is possible.[5,6] For simplicity, it is assumed that in the potential region between 0 – 0.3 V the dominant Mo surface form is $Mo(OH)_3$ at 0.311 V < E < 0.55 V MoO_2 and at E > 0.55 V MoO_3 and MoO_4 or the corresponding oxy-hydrates.

Electrochemical oxidation of hydrogen-carbon monoxide mixtures. The quasi-steady state (1 mV/s) polarization curves of a 0.1 % CO/H_2 mixture on the three different PtMo bulk alloy surfaces and on Pt in 0.5 M H_2SO_4 at 333 K are shown in Fig. 6. In order to assure the equilibration of the electrode surfaces with CO prior to recording the polarization curve, the electrode potential was held at 0.1 V for 3000 s (see the insert of Fig. 7) at a rotation rate of 2500 rpm, followed by a potential scan from 0 V. The $Pt_{77}Mo_{23}$ surface exhib-

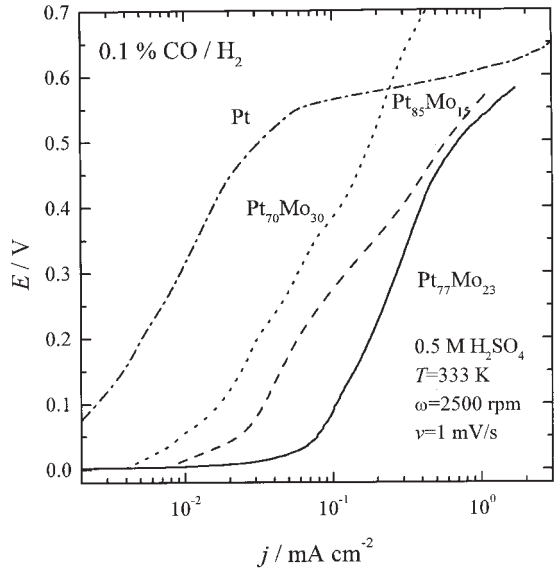

Fig. 6. Polarization curves (1 mV s^{-1}) for the oxidation of 0.1 % CO in hydrogen on different PtMo surfaces and pure Pt in 0.5 M H_2SO_4 at 2500 rpm, 333 K, followed by 3000 s poisoning at 0.1 V.

its the lowest overpotential for the oxidation of H_2 in the presence of 0.1 % CO, shifted negatively by 470 mV at an overpotential of 100 mV compared with a pure platinum electrode. The other two surfaces are less active but still both have a better activity than Pt, see Table II. The current density at 100 mV on a $Pt_{77}Mo_{23}$ surface is ≈ 0.1 mA cm^{-2}, which is a relatively small value, but taking into account that real fuel cell supported catalyst have a high surface area, this current should be multiplied by a factor of 300 which gives a current density of 30 mA cm^{-2} (notice that in real fuel cells, hydrogen is contaminated with 10 – 100 ppm of CO). The synergetic behavior of the PtMo alloys could be explained through a delicate balance between the number of bare platinum sites, which are required for the adsorption of molecular H_2, and the surface concentration of oxy-hydroxides which are required to oxidize CO_{ads} on Pt sites. $Pt_{70}Mo_{30}$ is the surface with the lowest activity because almost all the Pt surface atoms are covered with Mo surface oxy-hydroxides, as shown in the hydrogen oxidation experiments, so for one free Pt atom, a strong competition between CO, H_2 and OH from Mo occurs. A better activity is observed on $Pt_{85}Mo_{15}$ but the surface concentration of oxy-hydroxides is probably too small. Thus, the most active surface for the oxidation of H_2/CO mixtures is clearly the alloy having a surface composition close to 23 mol.% of Mo.

TABLE II. Potential at 0.1 mA cm^{-2} and current density at E = 0.1 V on different surfaces in a 0.1 % CO/H_2 mixture. (Data are taken from Fig. 7)

	E (j = 0.1 mA cm^{-2})/mV	j (E = 0.1 V)/μA cm^{-2}
Pt	565	2.5
$Pt_{85}Mo_{15}$	275	35
$Pt_{77}Mo_{23}$	94	104
$Pt_{70}Mo_{30}$	385	17.7

The insert in Fig. 7 shows the influence of the CO concentration in the H_2/CO mixtures on the electrode poisoning after switching from pure hydrogen to the H_2/CO mixtures. It can be seen that, contrary to pure platinum, the hydrogen oxidation reaction is not fully suppressed at 100 mV. A measurable steady state current was reached after ≈2000 s, while a pure platinum surface is completely poisoned after ≈100 s. The polarization curves taken after ≈3000 s of poisoning show that the mechanism of CO/H_2 oxidation reaction is complex. The highest reaction rate was observed near the hydrogen reversible potential, where a slope of ≈30 mV/dec was observed. Above 50 mV, the reaction rate is slower and the value of the slope is changed to ≈ 400 mV/dec, which could be attributed to a change of Mo oxidation state. It is obvious that decreasing the CO concentration increases the reaction rate. This observation is in agreement with the so-called "microshielding principle" mechanism.[15] In other words, the H_2 oxidation reaction occurs on the free sites liberated during the time between the oxidative removals of CO_{ads} and CO re-adsorption:

$$CO_{(sln)} \xrightarrow{k_{ads}} CO_{ads} \xrightarrow{OH, k_{ox}} CO_2 + H^+ + e^- \quad (11)$$

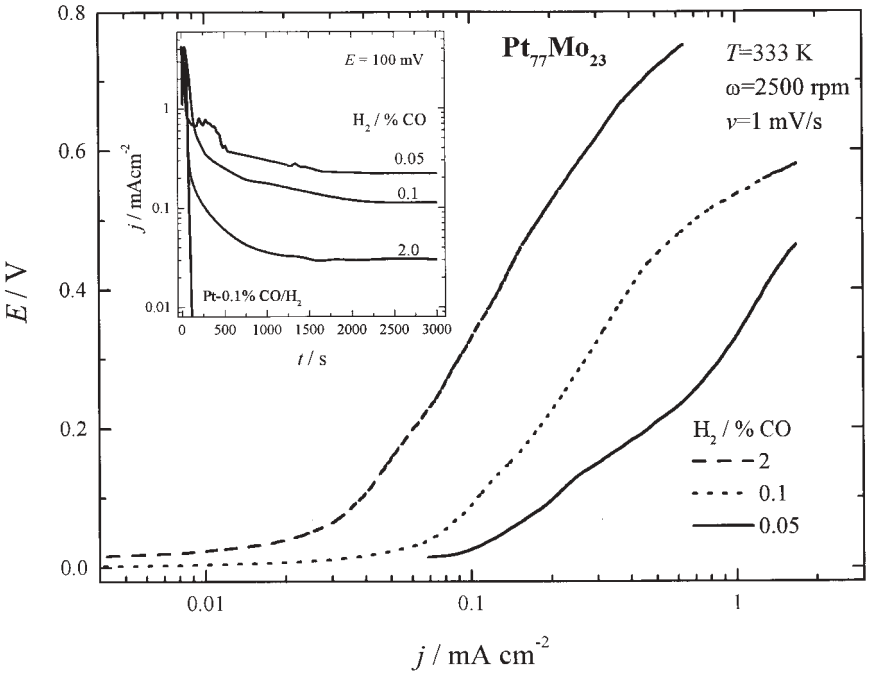

Fig. 7. Polarization curve for the oxidation of H_2 on the $Pt_{77}Mo_{23}$ alloy surface containing various levels of CO in 0.5 M H_2SO_4 at 2500 rpm, 333 K, after 3000 s of poisoning. Insert: Time dependance of the current density at 0.1 V at 2500 rpm following a switch from pure H_2 to H_2 containing different levels of CO on $Pt_{77}Mo_{23}$ and pure Pt.

Hence, the rate of the hydrogen oxidation reaction is faster when the level of CO in the mixtures is such that the flux to the surface is reduced to a point where the rate of CO oxidative removal from the surface far exceeds the rate of re-adsorption ($k_{ads} << k_{ox}$). Unfortunately, although PtMo is the best known catalyst to date for the CO/H_2 oxidation reaction, it seams that k_{ads} has a comparable or probably higher value than k_{ox} and so the current density for the H_2/CO oxidation in the low overpotential region is an order of magnitude smaller than that with pure hydrogen.

Mechanism of the oxidation CO/H_2 mixtures

Based on experimental evidence, the following mechanism of CO oxidation in the low potential region on a PtMo alloy could be given as follows:

$$CO + \text{Pt-Mo(OH)}_3 \underset{k_{des}(CO)}{\overset{k_{ads}(CO)}{\rightleftharpoons}} CO_{ads} - \text{Pt-Mo(OH)}_3 \qquad (12)$$

$$CO_{ads} - \text{Pt-Mo(OH)}_3 \underset{k_{red}(CO_2)}{\overset{k_{ox}(CO)}{\rightleftharpoons}} CO_2 + \text{Pt-Mo(OH)}_2 + H^+ + e^- \text{(rds)} \qquad (13)$$

$$\text{Pt-Mo(OH)}_2 + \text{H}_2\text{O} \underset{k_{\text{red}}}{\overset{k_{\text{ox}}}{\rightleftharpoons}} \text{Pt-Mo(OH)}_3 + \text{H}^+ + \text{e}^- \tag{14}$$

where: $k_{\text{ads}}(\text{CO})$ and $k_{\text{des}}(\text{CO})$ are the rate constants for CO adsorption and desorption, respectively; $k_{\text{ox}}(\text{CO})$ and $k_{\text{red}}(\text{CO}_2)$ are the rate constants for CO_{ads} oxidation and CO_2 reduction, respectively; k_{ox} and k_{red} are the rate constants for Mo(OH)_2 oxidation and Mo(OH)_3 reduction, respectively. As the rate determining (rds) reaction, Eq. (13) is proposed.

For steady state conditions, the change of CO_{ads} coverage in Eq. (13) can be given as:

$$-\frac{\partial\theta_{\text{CO}}}{\partial t} = k_{\text{ads}}(\text{CO})\frac{p(\text{CO})}{p^\circ}(1-\theta_{\text{CO}}-\theta_{\text{OH}}) - k_{\text{ox}}(\text{CO})\theta_{\text{CO}}\theta_{\text{OH}} = 0 \tag{15}$$

where $k_{\text{ox}}(\text{CO})$ is the potential dependent rate constant and p^{o} standard pressure:

$$k_{\text{ox}}(\text{CO}) = k^*_{\text{ox}}(\text{CO})\exp\left(\frac{\alpha FE}{RT}\right) \tag{16}$$

($k^*_{\text{ox}}(\text{CO})$ is the chemical rate constant and α is the transfer coefficient).

After rearranging Eq. (15) and neglecting $k_{\text{red}}(\text{CO}_2)$ and $k_{\text{des}}(\text{CO})$, the CO_{ads} coverage is:

$$\theta_{\text{CO}} = \frac{k_{\text{ads}}(\text{CO})[p(\text{CO})/p^\circ](1-\theta_{\text{OH}})}{k_{\text{ads}}(\text{CO})[p(\text{CO})/p^\circ] + k^*_{\text{ox}}(\text{CO})\theta_{\text{OH}}\exp\left(\frac{\alpha FE}{RT}\right)} \tag{17}$$

Considering the simple site-blocking model,[16] the poisoning of H_2 by adsorbed CO is given by:

$$j = j(\text{H}_2)(1-\theta_{\text{CO}})^n \tag{18}$$

where j is the measured current in the presence of CO, $j(\text{H}_2)$ is the current for pure H_2 oxidation. By substituting θ_{CO} from (17) into (18) one obtains:

$$j = j(\text{H}_2)\left\{1 - \frac{k_{\text{ads}}(\text{CO})[p(\text{CO})/p^\circ](1-\theta_{\text{OH}})}{k_{\text{ads}}(\text{CO})[p(\text{CO})/p^\circ] + k^*_{\text{ox}}\theta_{\text{OH}}\exp(\alpha FE/RT))}\right\}^n \tag{19}$$

where n, depending on the hydrogen oxidation mechanism, is 1 for a slow Heyrowsky reaction or 2 for a slow Tafel reaction. Equation (19) only qualitatively describes the polarization curve for the oxidation of H_2/CO mixtures, as can be seen from Fig. 8, where the simulation of Eq. (19) is given. The quantitative equation should include the coverage dependence of $k_{\text{ads}}(\text{CO})$, and the potential dependence of the different forms of Mo oxy-hydroxides, some of which are active and other are not for the CO oxidation reaction, but unfortunately this data are unknown at present.

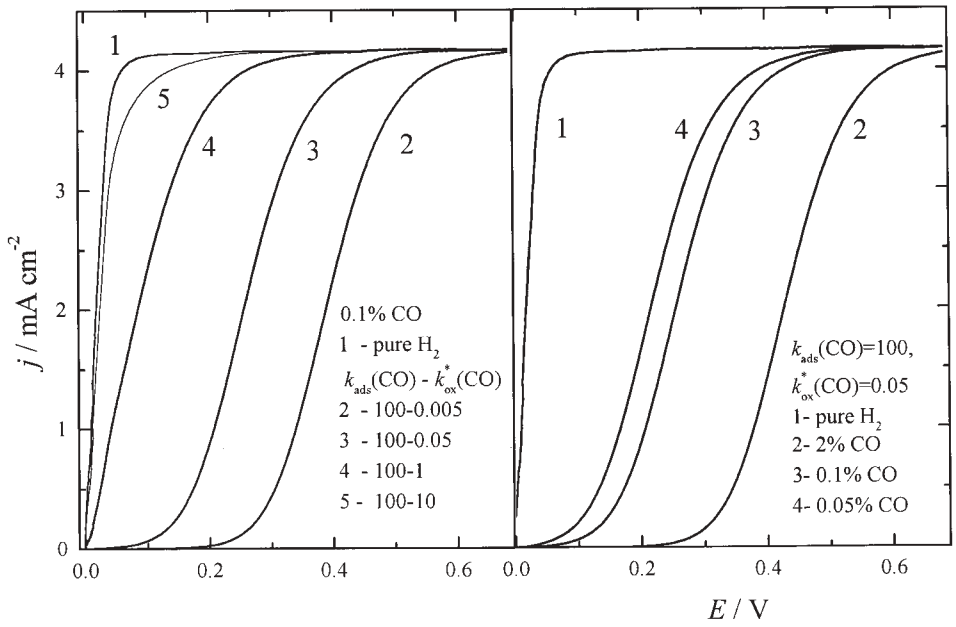

Fig. 8. Simulation of Eq. (19) left: for 0.1 % CO in hydrogen for k_{ads}(CO) = 100 s^{-1} and different values of k^*_{ox}(CO) in the range between 0.005 and 10 s^{-1}. Right: Simulation of Eq. (19) for 2, 0.1 and 0.05 % CO in hydrogen for k_{ads} (CO) = 100 s^{-1} and k^*_{ox}(CO) = 0.05 s^{-1}. In both cases $\alpha = 0.5$, $n = 2$, $\omega = 2500$ rpm and $T = 333$ K.

For the simulation of Eq. (19), the data for the pure hydrogen oxidation reaction on $Pt_{77}Mo_{23}$ (Fig. 5) was taken as $j(H_2)$, curve 1. The value for k_{ads}(CO) was taken to be 100 s^{-1} and k_{ox}^*(CO) was varied in the range between 0.005 and 10 s^{-1}. The partial pressure of CO was taken to be 0.001 (0.1 %), $\theta_{OH} = 0.05$ and $n = 2$. The simulation of Eq. (19) for different ratios of k_{ads}(CO) and k_{ox}^*(CO) is shown in Fig. 8 left. As can be seen, when k_{ox}^*(CO) has a comparable value, to k_{ads}(CO), curve 5, the polarization curve is almost identical to that for pure H_2 oxidation. On the other hand, when k_{ox}^*(CO) is 2000 times smaller (0.05 s^{-1}) than k_{ads}(CO), the polarization curve is the similar to the experimentally observed one (note: by the same analysis on pure Pt k_{ox}^*(CO) was $\approx 10^7$ times smaller). The influence of the CO partial pressure was simulated for three different CO concentrations in the hydrogen fuel for k_{ox}^*(CO) = 0.05 s^{-1}. The results are shown in Fig. 8 right. The similarity with the experimentally observed data is obvious.

From the given analysis, it can be concluded that the value of k_{ox}^*(CO) is the determining factor for the CO oxidation mechanism, because the values of the rate constant of CO adsorption are similar for the platinum alloys and pure platinum.[14] On the other hand, the rate of CO oxidation in (13):

$$\upsilon_{ox} = k_{ox}(\mathrm{CO})\,\theta_{OH}\theta_{CO} \tag{20}$$

includes the coverage of the active oxy-hydroxide species:

$$\theta_{OH} = \frac{a_s[Mo(OH)_3]}{a_s[Mo(OH)_3] + a_s[Mo(OH)_2]} \tag{21}$$

where a_s is the surface activity (*note*: Eq. (21) should include all the active and inactive oxy-species present and their potential dependencies).

Equation (21) directly determines the potential at which the alloys start to oxidize CO:

$$E_r[Mo(OH)_3|Mo(OH)_2] = E^0f[Mo(OH)_3|Mo(OH)_2] + \\ + \frac{RT}{f} \ln \frac{a_s[Mo(OH)_3]a(H^+)}{a_s[Mo(OH)_2]a(H_2O)} \tag{22}$$

($E^o_f[Mo(OH)_3|Mo(OH)_2]$ is the standard formal potential for reaction (14)):

$$\theta_{OH} = \left\{1 + \frac{a(H^+)}{a(H_2O)} \exp\left[-\frac{F(E_r - E_f^\circ)}{RT}\right]\right\} \tag{23}$$

Equation (23) can explain the difference in the activities of different platinum alloy catalysts (*e.g.*, PtSn compared with PtRu).

To have a compete picture of the complexity of the CO oxidation reaction, the coverage dependencies of the rate constants for the CO adsorption reaction should be included in Eq. (19):

$$k_{ads}(\theta_{CO}) = k\,P(\theta_{CO}) \exp\left(-\frac{\Delta_{ads}G^*(CO) + \gamma\Delta[\Delta_{ads}G(\theta_{CO})]}{RT}\right) \tag{24}$$

where k is the constant, $P(\theta_{CO})$ is the coverage dependent sticking probability of CO adsorption, $\Delta_{ads}G^*(CO)$ the Gibbs energy of adsorption for $\theta_{CO} = 0$, γ the symmetry of the activation barrier, and $\Delta[\Delta_{ads}G^*(\theta_{CO})]$ the coverage dependent part of the Gibbs energy of adsorption. This equation includes the existence of weakly adsorbed states of CO, when θ_{CO} is higher than 0.8 (see Ref. 1). Under the experimental conditions in this work, no conclusions could be reached about the existence of weakly adsorbed states of CO on PtMo. Recently. Bultrashat[17] *et al.* using DMSO (differential electrochemical mass spectrometry) showed that underpotentially deposited Mo on Pt is able to oxidize only ≈ 10 to 15 % of adsorbed CO at low potentials ($E < 0.4$ V), which they attributed to the oxidation of weakly adsorbed states of CO.

By including Eqs. (22) and (23) in (19), the complete equation for the CO/H_2 oxidation reaction, which cannot be solved because of numerous unknown parameters, can be obtained.

Aknowledgment: This work was supported by the Assistant Secretary for Energy Efficiency and Renewable Energy, Office of Transportation Technology, of the U.S. Department of Energy under Contract DE-AC03-76SF00098 and by the Ministry of Science, Technology and Development of Serbia, Contract No's: X-1796 and X-1825.

ИЗВОД

ЕЛЕКТРОХЕМИЈСКА ОКСИДАЦИЈА УГЉЕН-МОНОКСИДА: ОД МОНОКРИСТАЛА ПЛАТИНЕ ДО КАТАЛИЗАТОРА ЗА НИСКОТЕМПЕРАТУРНЕ ГОРИВНЕ ГАЛВАНСКЕ СПРЕГОВЕ. II ДЕО: ЕЛЕКТРОХЕМИЈСКА ОКСИДАЦИЈА H_2, CO И H_2/CO СМЕША НА ОКАРАКТЕРИСАНИМ PtMo ЛЕГУРАМА

БРАНИМИР Н. ГРГУР[1], НЕНАД М. МАРКОВИЋ[2] и PHILIP N. ROSS Jr[2]

[1]Технолошко-металуршки факултет, Универзитет у Београду, Карнегијева 4, 11001 Београд и [2]Lawrence Berkeley National Laboratory, 1 Cyclotron Road, MS 2-100, Berkeley, CA 94720, USA

Испитивана је оксидација водоника и његових смеша са угљен-моноксидом на површински окарактерисаним платина–молибден легурама припремљеним металуршким третманом. Закључено је да је оптимална површинска концентрација око 23 мол.% молибдена. На основу експериментално одређених параметара и симулације дискутован је механизам оксидације CO/H_2 смеша.

(Примљено 5. новембра 2002)

REFERENCES

1. B. N. Grgur, N. M. Marković, C. A. Lucas, P. N. Ross Jr, *J. Serb. Chem. Soc.* **66** (2001) 785
2. M. Watanabe, S. Mooto, *J. Electroanal. Chem.* **60** (1975) 267
3. B. N. Grgur, N. M. marković, P. N. Ross, *Electrochim. Acta* **24** (1998) 3631
4. R. Masel, *Principles of Adsorption and Reaction on Solid Surfaces*, Wiley, New York, 1996
5. M. Purbaix, *Atlas of Electrochemical Equilibria in Aqueous Solutions*, Pergamon Press, Oxford, 1966
6. *Encyclopedia of Electrochemistry of the Elements*, Vol. 5, Allen J. Bard, Ed., M. Dekker, New York, 1973
7. N. Marković, A. Widelov, P. Ross, O. Montero, I. Brown, *Cat. Lett.* **43** (1997) 161
8. I. Brown, X. Godechot, K. M. Yu, *Appl. Phys. Lett.* **58** (1991) 1392
9. J. Riviere, *Surface Analytical Techniques*, Oxford University Press, Oxford UK, 1990
10. W. Pearsons, *A Handbook of Lattice Spacings and Structures of Metals and Alloys*, Pergamon Press, London, 1958
11. P. N. Ross, *J. Vac. Sci. Technol.* **10** (1992) 2546
12. A. Miedema, A. Niessen, *Physica B&C* **114B** (1980) 367
13. B. N. Grgur, N. M. Marković, P. N. Ross, *J. Electrochem. Soc.* **5** (1999) 1613
14. H. A. Gasteiger, N. M. Marković, P. N. Ross, *J. Phys. Chem.* **99** (1995) 8290
15. H. A. Gasteiger, N. M. Marković, P. N. Ross, *Cat. Lett.* **36** (1996) 1
16. W. Vogel, J. Landquist, P. Ross, P. Stonehart, *J. Electroanal. Chem.* **20** (1975) 79
17. G. Samjeské, H. Wang, T. Loöffler, H. Baltruschat, *Electrochim. Acta* **47** (2002) 3681.